



**HAL**  
open science

## Downscaling MODIS-derived maps using GIS boosted regression trees: the case of frost occurrence over the arid Andean highlands of Bolivia

Robin Pouteau, Serge Rambal, Jean-Pierre Ratte, Fabien Gogé, Richard Joffre, Thierry Winkel

### ► To cite this version:

Robin Pouteau, Serge Rambal, Jean-Pierre Ratte, Fabien Gogé, Richard Joffre, et al.. Downscaling MODIS-derived maps using GIS boosted regression trees: the case of frost occurrence over the arid Andean highlands of Bolivia. *Remote Sensing of Environment*, 2011, 115 (1), pp.117-129. 10.1016/j.rse.2010.08.011 . ird-00543818

**HAL Id: ird-00543818**

**<https://ird.hal.science/ird-00543818>**

Submitted on 6 Dec 2010

**HAL** is a multi-disciplinary open access archive for the deposit and dissemination of scientific research documents, whether they are published or not. The documents may come from teaching and research institutions in France or abroad, or from public or private research centers.

L'archive ouverte pluridisciplinaire **HAL**, est destinée au dépôt et à la diffusion de documents scientifiques de niveau recherche, publiés ou non, émanant des établissements d'enseignement et de recherche français ou étrangers, des laboratoires publics ou privés.

1 **Downscaling MODIS-derived maps using GIS and boosted regression trees:**  
2 **the case of frost occurrence over the arid Andean highlands of Bolivia**

3

4 **Pouteau R., Rambal S., Ratte J.P., Gogé F., Joffre R., Winkel T.**

5

6

7 **Authors' addresses and affiliations**

8 Robin Pouteau (a, b), Serge Rambal (b), Jean-Pierre Ratte (b), Fabien Gogé (b), Richard Joffre (a, b),  
9 Thierry Winkel (a)

10 (a) IRD, CEFE-CNRS, F-34293 Montpellier cedex 5, France

11 (b) UMR 5175, CEFE-CNRS, F-34293 Montpellier cedex 5, France

12

13 **Corresponding author**

14 Thierry Winkel

15 IRD, CEFE-CNRS, F-34293 Montpellier cedex 5, France

16 E-mail: [thierry.winkel@ird.fr](mailto:thierry.winkel@ird.fr)

17

18 **Citation**

19 Pouteau R., Rambal S., Ratte J.P., Gogé F., Joffre R., Winkel T. 2011. Downscaling MODIS-derived  
20 maps using GIS and boosted regression trees: the case of frost occurrence over the arid Andean  
21 highlands of Bolivia. *Remote Sensing of Environment*, 115 (1): 117-129.

22 DOI: 0.1016/j.rse.2010.08.011

23

24 **Abstract**

25 Frost risk assessment is of critical importance in tropical highlands like the Andes where human  
26 activities thrive at altitudes up to 4200 m, and night frost may occur all the year round. In these semi-  
27 arid and cold regions with sparse meteorological networks, remote sensing and topographic modeling  
28 are of potential interest for understanding how physiography influences the local climate regime. After  
29 integrating night land surface temperature from the MODIS satellite, and physiographic descriptors  
30 derived from a digital elevation model, we explored how regional and landscape-scale features  
31 influence frost occurrence in the southern altiplano of Bolivia. Based on the high correlation between  
32 night land surface temperature and minimum air temperature, frost occurrence in early-, middle- and  
33 late-summer periods were calculated from satellite observations and mapped at a 1-km resolution over  
34 a 45000 km<sup>2</sup> area. Physiographic modeling of frost occurrence was then conducted comparing multiple  
35 regression (MR) and boosted regression trees (BRT). Physiographic predictors were latitude, elevation,  
36 distance from salt lakes, slope steepness, potential insolation, and topographic convergence. Insolation  
37 influence on night frost was tested assuming that ground surface warming in the daytime reduces frost  
38 occurrence in the next night. Depending on the time period and the calibration domain, BRT models  
39 explained 74% to 90% of frost occurrence variation, outperforming the MR method. Inverted BRT  
40 models allowed the downscaling of frost occurrence maps at 100-m resolution, illustrating local  
41 processes like cold air drainage. Minimum temperature lapse rates showed seasonal variation and  
42 mean values higher than those reported for temperate mountains. When applied at regional and  
43 subregional scales successively, BRT models revealed prominent effects of elevation, latitude and  
44 distance to salt lakes at large scales, whereas slope, topographic convergence and insolation gained  
45 influence at local scales. Our results highlight the role of daytime insolation on night frost occurrence at  
46 local scale, particularly in the early- and mid-summer periods when solar astronomic forcing is  
47 maximum. Seasonal variations and interactions in physiographic effects are also shown. Nested effects  
48 of physiographic factors across scales are discussed, as well as potential applications of physiographic  
49 modeling to downscale ecological processes in complex terrains.

50

51 **Key words**

52 altiplano; Andes; Bolivia; boosted regression trees; DEM; downscaling; frost risk mapping; MODIS;  
53 physiography; temperature lapse rate; topoclimate model; satellite land surface temperature; seasonal  
54 variation; spatial variation

55

56

## 57 1. Introduction

58 Low air temperature is one of the most important factors controlling vegetation zonation and key  
59 processes such as evapotranspiration, carbon fixation and decomposition, plant productivity and  
60 mortality in natural and cultivated mountain ecosystems (Chen et al., 1999; Nagy et al., 2003).  
61 Depending on vegetation structure, landscape position or soil properties, frost can damage plant tissues  
62 thus affecting forest, pasture and crop productivity (Blennow & Lindkvist, 2000). These damages have  
63 consequences for human populations, particularly in the tropics where highlands often remain densely  
64 populated (Grötzbach & Stadel, 1997). In the Andes of Argentina, Bolivia, Chile, Ecuador and Peru  
65 agriculture thrives at altitudes up to 4200 m (Del Castillo et al., 2008) and treeline reaches its world's  
66 highest elevation up to 5100 m (Hoch & Körner, 2005) in spite of night frost occurring on more than 300  
67 days practically spread all over the year (Garcia et al., 2007; Gonzalez et al., 2007; Rada et al., 2009;  
68 Troll, 1968). In the southern Andes, sparsely vegetated areas juxtaposing extended flat plains around  
69 salt lakes and steep slopes on the cordilleras and volcanos, display semi-arid and desert landscapes  
70 largely dominated by terrain structure. Subjected to the night/day and sunlit/shaded slope contrasts  
71 characteristic of the mountain climate, this environment is well suited for examining the influence of  
72 regional and landscape-scale physiography on the local climate regime, and particularly frost  
73 occurrence.

74 Several studies on topoclimate in highlands showed that elevation and slope are the main  
75 explanatory variables in modeling local climate spatial variability (Chuanyan et al., 2005). By means of  
76 digital elevation models and astronomical equations, the potential insolation (incoming solar radiation)  
77 has been included as an additional independent variable in some of these models, substantially  
78 improving their capacity to predict free-air as well as soil-surface temperature distributions (Benavides  
79 et al., 2007; Blennow & Lindkvist, 2000; Fridley 2009; Fu & Rich, 2002). Among the physiographic  
80 variables, elevation and slope steepness are known to influence cold air drainage at night and, hence,  
81 the distribution of frost risks at landscape scale (Lundquist et al., 2008; Pypker et al., 2007a). In the  
82 daytime, slope aspect and physiographic shading effects control the effective radiation load per unit of  
83 soil areas, resulting in very contrasted values of daily maximum soil temperature (Fu & Rich, 2002).  
84 Minimum night temperature might be sensitive to insolation during the previous day, since soil surface  
85 warming during that day could dampen soil radiative cooling in the next night. Though challenged by  
86 studies on minimum air temperature variations in moderately high mountains under temperate climate  
87 (Blennow 1998; Dobrowski et al., 2009), this hypothesis should be tested in the central part of the  
88 Andes, where low latitude, high elevation (typically ranging between 3600 and 4200 m) and sparse  
89 vegetation result in much greater radiation load and thermal contrasts across shaded and sunlit areas.  
90 Besides, using a downscaling approach, Fridley (2009) noticed that the lack of relationship between  
91 daytime radiation and nighttime temperature is true at local scale lower than 1000 m but not at regional  
92 scale (Great Smoky Mountains, USA), where variations in radiation balance across locations do  
93 influence nighttime temperature distribution particularly in cooler situations. Considering the Andes,  
94 recent work by Bader & Ruijten (2008) and Bader et al. (2008) used topographic modeling and remote  
95 sensing data to examine the response of vegetation distribution to climate warming, but we should go  
96 back to Santibañez et al. (1997) and François et al. (1999) to find studies on the links between frost

97 climatology and physiography over this region. These early works were not continued, and the case of  
98 the Andean highlands remained poorly documented in spite of the potential interest of that region,  
99 densely populated and representative of the tropical mountains vulnerable to global warming (Vuille et  
100 al., 2008).

101 Analyzing topographic effects on free-air or land surface temperature also led to reevaluate the  
102 simplifying assumption of a generic environmental lapse rate (the decrease in free-air temperature as  
103 elevation rises, typically assumed to be  $-0.6\text{ }^{\circ}\text{C}$  per 100 m), commonly applied in hydrological and  
104 ecological studies to extrapolate air temperature in mountain areas. In fact, several studies show  
105 temperature lapse rate variations due to seasonality, height above the ground, or ground surface  
106 characteristics (Blandford et al., 2008; Dobrowski et al., 2009; Fridley 2009; Lookingbill & Urban, 2003;  
107 Marshall et al., 2007), though no detailed reports were published for the Central Andes.

108 Most of the above mentioned studies used multiple linear regression for modeling the influence of  
109 physiography on free-air or soil-surface temperatures. The present study resorts to an advanced form of  
110 regression, the boosted regression trees (BRT). BRT use the boosting technique to combine large  
111 numbers of relatively simple tree models to optimize predictive performance. BRT have been used  
112 successfully in human biology (Friedman and Meulman 2003), land cover mapping (Lawrence et al.,  
113 2004), biogeography (Parisien & Moritz, 2009), species distribution (Elith et al., 2008), and soil science  
114 (Martin et al., 2009). They offer substantial advantages over classical regression models since they  
115 handle both qualitative and quantitative variables, can accommodate missing data and correlated  
116 predictive variables, are relatively insensitive to outliers and to the inclusion of irrelevant predictor  
117 variables, and are able to model complex interactions between predictors (Elith et al., 2008; Martin et  
118 al., 2009). Though direct graphic representation of the complete tree model is impossible with BRT, the  
119 model interpretation is made easy by identifying the variables most relevant for prediction, and then  
120 visualizing the partial effect of each predictor variable after accounting for the average effect of the  
121 other variables (Friedman & Meulman, 2003).

122 The aims of the present work were: i) to explore how regional and landscape-scale physiography  
123 influence frost occurrence in Andean highlands through integration of field and remote sensing data,  
124 digital terrain analysis, and GIS, ii) to downscale regional frost occurrence maps at a level relevant for  
125 farming and land management decisions using BRT models. This study was focused on the austral  
126 summer period, from November to April, when frost holds the greatest potential impact for local farming  
127 activities.

## 128 **2. Material and methods**

### 129 *2.1. Study area and regional climate*

130 The study area was located at the southwest of the Bolivian highlands, near the borders of  
131 Argentina and Chile, between  $19^{\circ}15'$  and  $22^{\circ}00'$  South and between  $66^{\circ}26'$  and  $68^{\circ}15'$  West. This  
132 region, boarded by the western Andes cordillera, is characterized by the presence in its centre of a  
133 ca.100 x 100 km dry salt expanse, the Salar of Uyuni, while another salt lake, the Salar of Coipasa, lies  
134 at the north of the study area. The landscapes show a mosaic of three types of land units: more or less  
135 extended flat shores surrounding the salt lakes (elevation ca. 3650 m) and an alternation of valleys and

136 volcanic relieves (culminating at 6051 m) in the hinterland. The native vegetation of this tropical Andean  
137 ecosystem, also known as *puna*, consists of a mountain steppe of herbaceous and shrub species (e.g.  
138 *Baccharis incarum*, *Parastrephia lepidophylla*, and *Stipa spp.*) (Navarro & Ferreira, 2007) traditionally  
139 used as pastures but progressively encroached by the recent and rapid expansion of quinoa crop  
140 (*Chenopodium quinoa* Willd.) (Vassas et al., 2008).

141 Due to its low latitude and high elevation, the study area is characterized by a cold and arid tropical  
142 climate. Average precipitations vary between 100 and 350 mm year<sup>-1</sup> from the South to the North of the  
143 region (Geerts et al., 2006), presenting an unimodal distribution with a dry season from April to October.  
144 The annual average temperature (close to 9 °C) hides daily thermal amplitudes higher than seasonal  
145 amplitudes, of up to 25 °C (Frère et al., 1978). These particular thermal conditions lead to high frost  
146 risks throughout the year. Advections of air masses from the South Pole represent only 20% of the  
147 observed frosty nights (Frère et al., 1978) and are four times less frequent in the summer than during  
148 the winter, when the intertropical convergence zone goes northward (Ronchail, 1989). Therefore, the  
149 main climatic threat lies in radiative frost, occurring during clear and calm nights. As reported by local  
150 peasants, frost occurrence shows a strong topographical and orographical dependence, as well as a  
151 marked seasonality. This seasonality lead us to split the active vegetation period into three time periods  
152 characterizing the mean regional climate dynamics in the summer rainy season: November-December  
153 when precipitation and minimum temperature rise progressively, January-February when precipitation  
154 and temperature are at their maximum, and March-April when both begin to decrease.

## 155 2.2. Data

### 156 2.2.1. Meteorological ground data

157 In the study area, daily air temperature records were available in three meteorological stations: one  
158 at Salinas de Garci Mendoza (19°38'S, 67°40'W) managed by the SENAMHI (Meteorology and  
159 Hydrology National Service, Bolivia) where daily minimum air temperature (T<sub>n</sub>) was recorded in 1989  
160 and from 1998 to 2006, and two others at Irpani (19°45'S, 67°41'W) and Jirira (19°51'S, 67°34'W)  
161 where meteorological stations set up by the IRD (Research Institute for Development, France) recorded  
162 semi-hourly air temperature from 23 November 2005 to 18 February 2006 in Irpani, and from 6  
163 November 2006 to 31 December 2007 in Jirira. This dataset was temporally and spatially insufficient to  
164 interpolate frost risks at a regional scale, but it allowed to establish the relationship between air  
165 temperature and remotely sensed land surface temperature.

### 166 2.2.2. Remotely sensed data

167 The two sensors, Terra and Aqua, of the satellite system MODIS give daily images of the Earth  
168 radiative land surface temperature. Images from the fifth version of the MYD11A1 MODIS product were  
169 concatenated and projected in the UTM-19S (Universal Transverse Mercator 19 South) coordinate  
170 system using the MODIS projection tool. In this way, daily 1-km resolution images of the radiative land  
171 surface temperature (T<sub>s</sub>) over the study area were obtained. T<sub>s</sub> images recorded by the Aqua sensor  
172 around 2 a.m. were used as they were closer to the T<sub>n</sub> data recorded at ground level and closer to the  
173 true physiological conditions experienced by the vegetation (François et al., 1999). Time series of  
174 nominal 1-km spatial resolution MODIS data were downloaded from NASA's EOS data gateway

175 (<https://wist.echo.nasa.gov/>) from 20 July 2001 to 25 April 2006 and from 01 January 2007 to 31  
176 December 2007. Due to the particular surface properties of the salt lakes of Coipasa and Uyuni in terms  
177 of surface moisture and radiative emissivity, parameter estimations were considered dubious there and  
178 Ts data for the salt lakes were discarded from the analysis. This database was managed and analyzed  
179 using the ENVI 4.2. software (ITT Visual Information Solutions, [www.itvis.com](http://www.itvis.com)). The statistical  
180 correspondence between Tn data recorded in the meteorological stations of Salinas, Irpani and Jirira  
181 and Ts data of the pixels including these three localities was examined by linear regression and  
182 Pearson correlation.

183 Apart from Ts measurements during clear nights, MODIS images also bring information about the  
184 possible presence of clouds between the Earth surface and the satellite at the time of the record. The  
185 information of these “flagged” images is valuable for our purpose since radiative frost would not occur  
186 during cloudy nights. The frequency of cloudy pixels in the daily MODIS images was thus calculated  
187 and used in the frost occurrence calculation (see below).

### 188 *2.2.3. Digital elevation model and physiographic predictors*

189 The SRTM digital elevation model (Farr et al., 2007) with a 90 m horizontal resolution and a  
190 vertical accuracy better than 9 m was used after resampling to 100 m to make easier the  
191 correspondence between the digital elevation model and the MODIS images at 1-km scale. In a GIS  
192 environment using Idrisi Kilimanjaro, Envi 4.2. and ArcMap 9.2. softwares, eight physiographic variables  
193 were calculated at a 100-m resolution for each location to examine their potential role in the spatial  
194 determinism of frost and to downscale frost maps to levels closer to those of frost impacts on anthropic  
195 activities (Table 1). The compound topographic index (CTI) was used as an index of cold air drainage  
196 (Gessler et al., 2000), with low CTI values representing convex positions like mountain crests and with  
197 high CTI values representing concave positions like coves or hillslope bases. Three insolation variables  
198 (DPI, MPI and API) were calculated by the ArcMap 9.2. solar analysis tool. They express the amount of  
199 radiative energy received across all wavelengths over the course of a typical seasonal day (DPI), or  
200 from sunrise to 12:00 (MPI), or from 12:00 to sunset (API) of such a day.

201 These insolation variables account for site latitude and elevation, slope steepness and aspect,  
202 daily and seasonal sun angle, and shadows cast by surrounding heights. API was calculated to  
203 examine the specific influence of insolation in the afternoon just before the considered night, with the  
204 hypothesis that high soil surface insolation and warming would affect the soil energy balance, and thus  
205 reduce the risk of radiative frost in the following night (without regards to other potential factors such as  
206 soil albedo, soil water content, air humidity, etc. see Garcia et al. (2004)). Similarly, MPI was calculated  
207 as a surrogate to the early morning insolation, with the hypothesis that areas in the shade of  
208 surrounding heights in the early morning would experience cooler conditions for a longer time, thus  
209 being more vulnerable to frost than sunlit areas. In the calibration procedure, these 100-m resolution  
210 variables were upscaled at 1-km resolution by averaging 10 x 10 pixel clusters in the DEM 100-m  
211 images, thus fitting the 1-km resolution of the remotely sensed frost occurrence maps.

212

213

214 **Table 1.** Ranges of physiographic variables observed over the study area.

Variable	Minimum	Maximum	Unit
LAT latitude in UTM 19 South	-22.00	-19.24	decimal degree
ELE elevation	3540	6051	m
SLO slope steepness	0	35	degree
DPI daily potential insolation			
Nov-Dec	6900	9075	W m <sup>-2</sup>
Jan-Feb	7040	8935	W m <sup>-2</sup>
Mar-Apr	4604	7897	W m <sup>-2</sup>
MPI morning potential insolation			
Nov-Dec	510	1861	W m <sup>-2</sup>
Jan-Feb	466	1772	W m <sup>-2</sup>
Mar-Apr	264	1240	W m <sup>-2</sup>
API afternoon potential insolation			
Nov-Dec	2819	5075	W m <sup>-2</sup>
Jan-Feb	2816	5000	W m <sup>-2</sup>
Mar-Apr	2079	4308	W m <sup>-2</sup>
LDS distance from salt lakes	0	5.04	Ln (km + 1)
CTI compound topographic index	5.7	14.1	-

215

216 *2.3. Physiographic modeling of frost occurrence over regional and subregional domains*

217 *2.3.1. MODIS-derived frost occurrence*

218 Frost is detected by remote sensing when surface temperature appears negative on cloudfree  
 219 images. Based on the standard meteorological threshold of 0 °C, frost occurrence (R) for a specific time  
 220 period was therefore defined as follows:

221

222  $R = Prob(T_s < 0\text{ }^{\circ}\text{C}) * F$  (1)

223

224 where: R = frost occurrence at the 0 °C threshold (relative probability ranging from 0 to 1), *Prob* ( $T_s < 0$   
 225 °C) = probability of the surface radiative temperature being lower than 0°C, F = frequency of cloudless  
 226 days in the considered period. Note that “frost occurrence” is used here instead of frost risk to  
 227 differentiate our estimates based on 6-year daily  $T_s$  values from climatological estimates based on  
 228 longer data series.

229 In order to calculate the probability *Prob* ( $T_s < 0\text{ }^{\circ}\text{C}$ ), the distribution of the random variable  $T_s$   
 230 during successive time periods (namely: November-December, January-February, March-April) was  
 231 studied, checking its normality through the Kolmogorov-Smirnov test. For each 1-km pixel and each  
 232 time period,  $T_s$  mean and standard deviation, cloudless day frequency (F) and, finally, frost occurrence



233 (R) were calculated from the available nighttime remotely sensed data series (n = 366 , 355, and 361 in  
234 the ND, JF and MA periods respectively). Maps of observed (remotely sensed) frost occurrence at 1-km  
235 resolution were then generated by applying Eq. (1) for each time period.

### 236 2.3.2. Frost occurrence models over regional and subregional domains

237 A subsample of 1-km pixels (n = 7500) was randomly selected for the calibration of the  
238 physiography-frost occurrence relationships over the entire study area (hereafter called "regional  
239 models"). Regional BRT were built for each seasonal period (November-December, January-February,  
240 March-April) using the *gbm* package version 1.6-3 developed under R software (R Development Core  
241 Team 2006). A bag fraction of 0.5 was used which means that, at each step of the boosting procedure,  
242 50% of the data in the training set were drawn at random without replacement. The loss function (LF),  
243 defining the lack-of-fit, used a squared-error criterion. The learning rate or shrinkage parameter (LR),  
244 the tree size or tree complexity (TS), the number of trees (NT) and the minimal number of observations  
245 per terminal node (MO) were the main parameters for these fittings, and were set through a tuning  
246 procedure (Martin et al., 2009). LR, determining the contribution of each tree to the model, was thus  
247 taken equal to 0.05. NT, the maximal number of trees for optimal prediction was set to 2000. For  
248 optimal prediction, TS, the maximal number of nodes in the individual trees, was set to a value of 9, and  
249 MO was set to 10 observations per terminal node. For sake of comparison, multiple linear regression  
250 models were calculated at the regional scale using the same predictors and the same calibration  
251 datasets as for the regional BRT. These " regional MR" were built using the Statistica package (StatSoft  
252 France 2005).

253 The regional BRT and MR models were validated comparing observed (remotely sensed) and  
254 predicted frost occurrence over the entire study area in the three time periods. This was made  
255 excluding the pixels used for calibration, which resulted in a 49353 pixels validation set. The predictive  
256 capacity of the models was analysed examining the observed versus predicted values plots, the bias  
257 (B), the root mean square error of prediction (RMSE), and the coefficient of determination of the  
258 regression between estimated and observed values ( $R^2$ ). Once validated, the BRT were interpreted,  
259 looking first at the relative contribution of the physiographic variables to the predictive models, and then  
260 considering the partial dependence of the predictions on each variable after accounting for the average  
261 effect of the other variables.

262 In order to test the scale-dependence of the predictors, a similar BRT procedure was applied over a  
263 smaller spatial domain defined by a selected range of regionally varying factors, namely: latitude  
264 between 19°5 and 20° South and elevation lower than 4200 meters (total area = 7775 km<sup>2</sup>). This spatial  
265 domain corresponds to the *Intersalar*, the area of major agricultural activities in the region, where local  
266 populations cultivate quinoa and rear camelids up to an altitude of ca. 4200 meters. A new set of 7500  
267 training pixels was randomly selected from this smaller domain to calibrate these "subregional BRT",  
268 using the same values of fitting parameters and a similar validation procedure as in the previous  
269 analysis. Excluding the training pixels, this validation was conducted on the remaining 275 pixels of this  
270 smaller domain. The relative contribution of the physiographic predictors to the subregional models was

271 also examined. The interactions between predictive variables were considered by joint plots of their  
272 partial dependence in the subregional models.

### 273 2.3.3. Downscaling frost occurrence prediction at 100-m resolution

274 Once validated, the regional BRT were applied on each pixel of the DEM 100-m image in order to  
275 downscale frost occurrence from 1-km to 100-m resolution in the three considered time periods. An  
276 indirect validation of these 100-m frost occurrence maps was then conducted by aggregating 10 x 10  
277 pixel clusters of 100-m frost predictions and comparing the resulting 1-km predictions to the observed  
278 (remotely sensed) frost occurrence at 1-km resolution. A qualitative validation was also conducted by  
279 examining the capacity of these 100-m maps to display well-known local patterns of frost and cold air  
280 distribution over complex terrains.

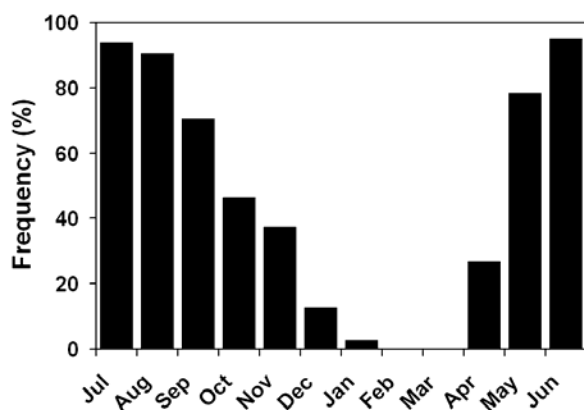
### 281 2.3.4. Estimation of the land surface temperature lapse rate

282 The regression of  $T_s$  recorded over sloping areas *versus* elevation of the corresponding pixels  
283 allowed to calculate average values of the land surface temperature lapse rate at night for successive  
284 dates in each considered time periods. Sloping areas were defined as terrains with slope steepness  
285 greater than  $3^\circ$  and elevation lower than 5000 meters. This elevation limit was chosen to discard high-  
286 altitude sites possibly covered with snow or ice which superficial thermal properties modify lapse rate  
287 estimations (Marshall et al., 2007). The resulting sampling area represented 22529 km<sup>2</sup>, covering an  
288 elevation range of 1341 m (from 3659 to 5000 m).

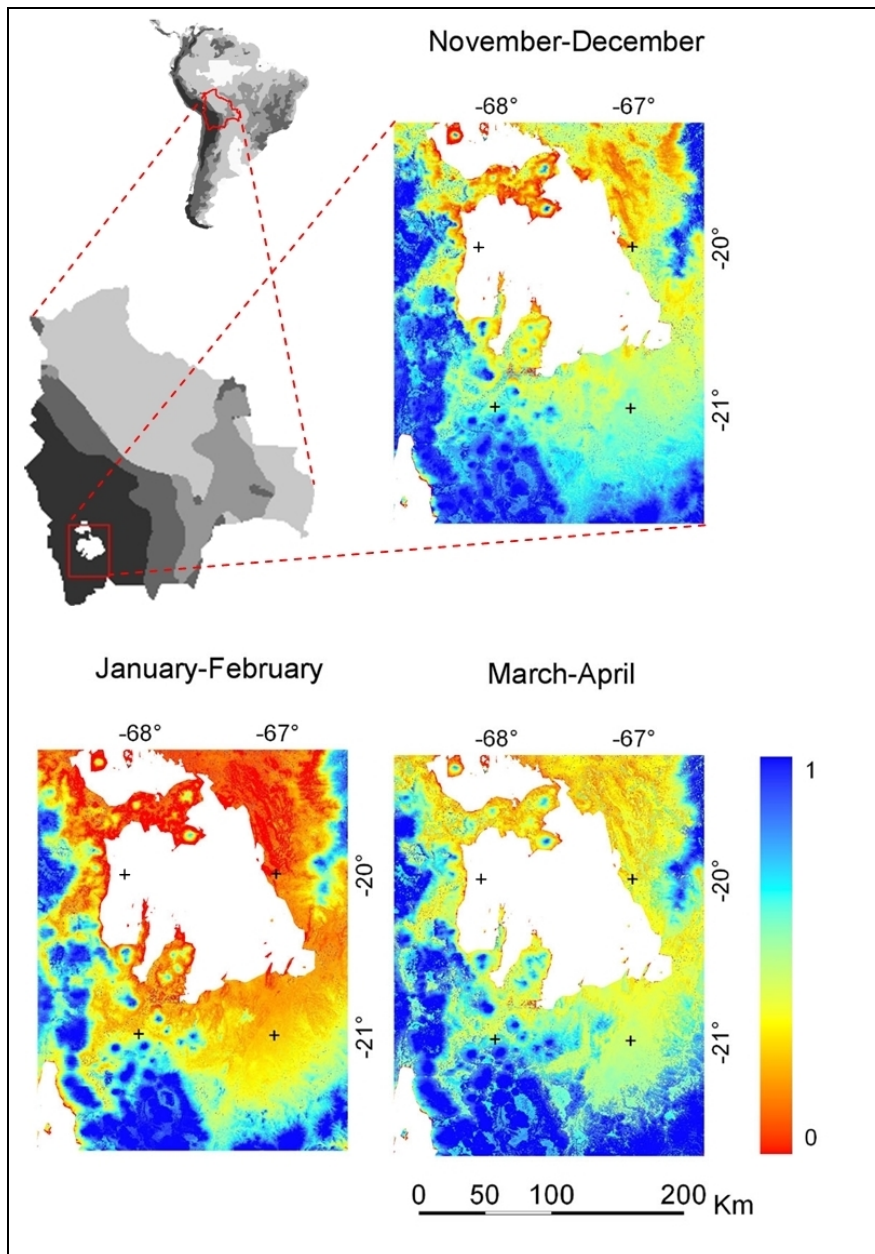
## 289 3. Results

### 290 3.1. Climate information and remotely sensed frost occurrence evaluation

291 The frequency analysis of daily minimum air temperature ( $T_n$ ) recorded at Salinas over 10  
292 discontinuous years (1989, and the 1998-2006 period) was made using the standard climatological  
293 threshold of  $0^\circ\text{C}$  (Fig. 1).



294  
295 **Fig. 1.** Frequency analysis of daily minimum air temperatures lower than  $0^\circ\text{C}$  registered at Salinas in  
296 1989 and from 1998 to 2006.



297

298 **Fig. 2.** One-kilometer resolution maps of MODIS-derived frost occurrence in southern Bolivia in three  
 299 successive time periods (the color scale at the right shows the frost probability)

300 During the austral summer (November-April), two periods of frequent below zero temperatures  
 301 surround a ca. 80-day time interval of low frost occurrence, from the beginning of January to the end of  
 302 March.

303 Daily  $T_n$  values recorded at screen height by the meteorological stations of Salinas, Irpani and Jirira  
 304 were highly correlated to  $T_s$  data remotely sensed over these three localities at night by the MODIS  
 305 satellite ( $T_n = 0.97 \cdot T_s + 0.93$ ,  $R^2 = 0.81$ ,  $n = 750$ ). The percentage of cloudy pixels on the MODIS  
 306 images gives a general information about the seasonal pattern of cloud cover in the study area: the  
 307 January-February period was the most overcast with on average  $46 \pm 8.2\%$  of the study area masked  
 308 by clouds in each daily satellite image, while this percentage fell to  $30 \pm 7.4\%$  and  $29 \pm 6.6\%$  in the  
 309 November-December and March-April periods respectively. The test of Kolmogorov-Smirnov applied to

310 the Ts data series was statistically significant in all the cases ( $P < 0.05$ ). This allowed to apply a normal  
311 probability density function in equation (1) in order to generate the 1-km resolution maps in Fig. 2  
312 showing the regional patterns of frost occurrence variations in three successive time periods as derived  
313 from satellite observations.

### 314 3.2. *Physiographic modeling of frost occurrence*

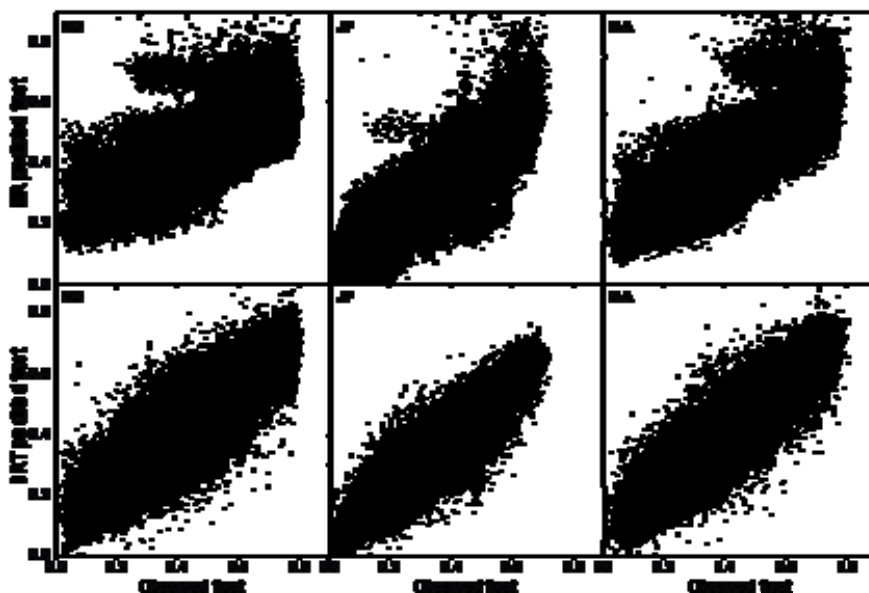
#### 315 3.2.1. *Model validation of regional and subregional BRT models*

316 The results of the statistical comparison between observed and predicted frost occurrence at 1-km  
317 resolution in three time periods are presented in Fig. 3 and Table 2. The regional BRT clearly  
318 outperformed the MR models, the latter being affected by strong non linearities in the high frost  
319 occurrence range, showing its poor predictive capacities in the early and late summer periods. On the  
320 other hand, the regional BRT negligibly overestimated the satellite observations with practically no bias  
321 whatever the time period. The RMSE and  $R^2$  values showed that BRT predictions were fairly good in  
322 January-February (RMSE = 0.057,  $R^2 = 0.90$ ), and only slightly more dispersed by the beginning or the  
323 end of the summer season (RMSE between 0.07 and 0.08,  $R^2$  between 0.78 and 0.83). With an error  
324 generally less than 8% on predicted frost occurrence values, the regional BRT thus appear suitable for  
325 predicting frost occurrence from physiographic variables alone. Table 2 shows similar performances of  
326 the regional and subregional BRT, with only higher bias for the subregional model.

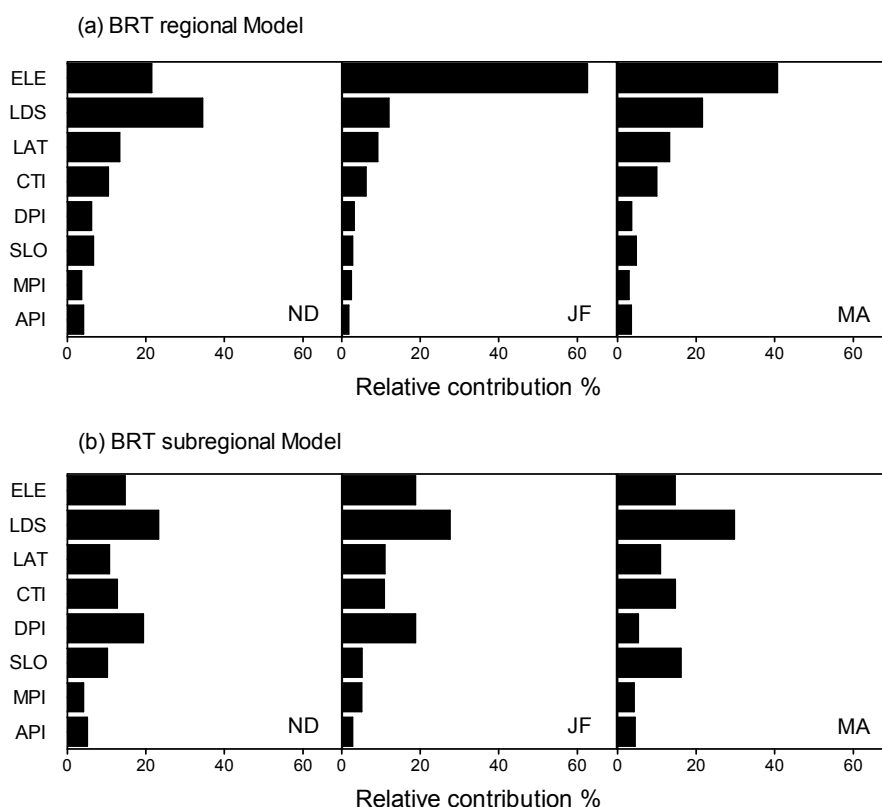
#### 327 3.2.2. *Hierarchy of physiographic variables in regional and subregional BRT*

328 Regional BRT showed large effects of elevation, distance from the salt lakes, latitude and CTI on  
329 frost occurrence, while slope and insolation variables had only marginal influence (Fig. 4a). Comparing  
330 the three time periods, the relative contributions of the predictive variables showed some variations,  
331 with the distance from the salt lakes dominating in the initial period (November-December), while  
332 elevation became more important from January to April, and particularly in the mid-summer period. In  
333 contrast, latitude, CTI and insolation variables kept a fairly constant effect with similar contributions at  
334 the beginning and at the end of the season. Calibrating BRT models over a limited spatial domain  
335 reveals slightly different patterns in the contributions of the predictors (Fig. 4b): distance from the salt  
336 lakes gained importance on elevation in the three time periods, and daily potential insolation showed  
337 noticeable contribution until mid-summer (though the influence of its morning and afternoon  
338 components remained marginal). The weights of CTI and latitude were intermediate whatever the time  
339 period, while the contribution of slope became important by the end of the season.

340



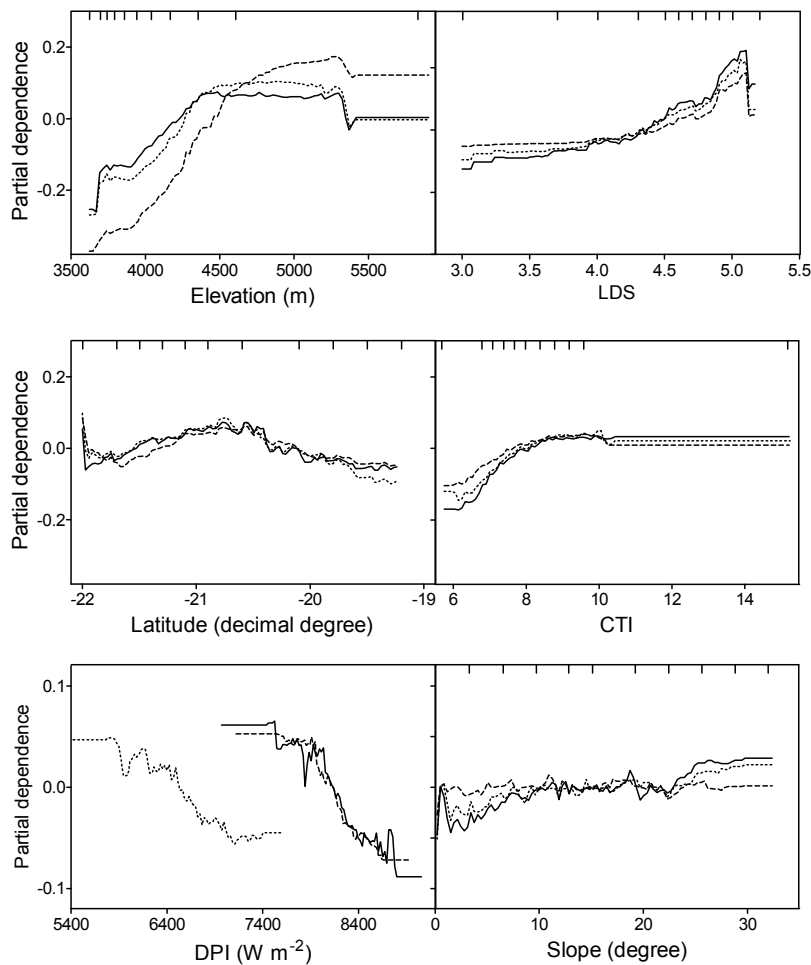
341  
 342 **Fig. 3.** Comparison of frost occurrence values observed in three time periods with frost occurrence  
 343 predicted by the MR (multiple regression) and BRT regional models (ND = November-December; JF =  
 344 January-February; MA = March-April, n = 49353 in each time period)



345  
 346 **Fig. 4.** Relative contributions of the physiographic variables in the regional (a) and subregional (b) BRT  
 347 in three time periods. (ND = November-December; JF = January-February; MA = March-April; see  
 348 Table 1 for variables abbreviations)

349 3.2.3. Partial dependence in regional and subregional BRT

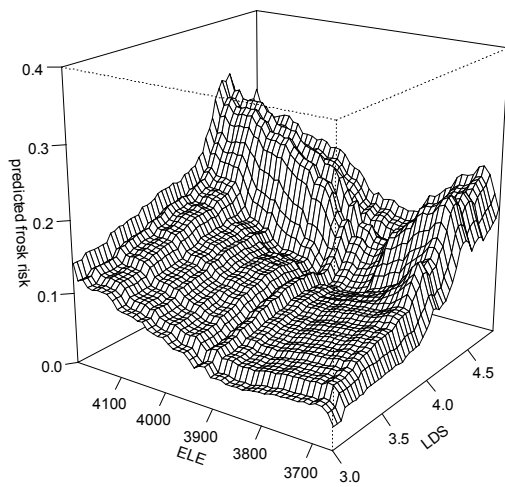
350 The plots of partial dependence for frost occurrence in the regional BRT (Fig. 5) indicate that frost  
351 events in the study area occur mostly at high and medium latitude, increase continuously up to 4500 m  
352 elevation, and are more frequent far away from the salt lakes. Concave positions (high CTI values) are  
353 more prone to frost, and low daily potential insolation in those shaded areas also increases frost  
354 occurrence at night, though separating the morning and afternoon components of the daily insolation  
355 gives opposite results (data not shown). The dependence of frost occurrence on slope steepness  
356 remained fairly constant. These partial responses of frost occurrence to the most active physiographic  
357 variables show only limited seasonal changes.



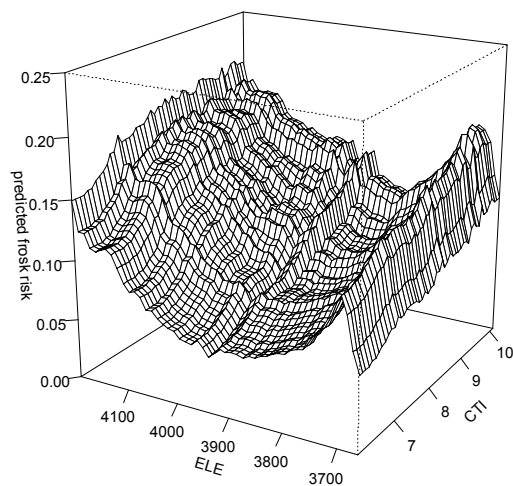
358 **Fig. 5.** Partial dependence plots of the six most influential physiographic variables in the regional BRT  
359 in three time periods (continuous line: November-December, dashed line: January-February, dotted  
360 line: March-April; ticks at the inside top of the plots show deciles of site distribution across the variable;  
361 see Table 1 for variables abbreviations).  
362

363 More details emerge from the partial dependence plots of interactions in subregional BRT (Fig. 6  
364 illustrating the January-February period, with similar results in the other two periods). For instance, up  
365 to a distance of 10 km from the salt lakes (LDS  $\approx$  4.0) the effect of elevation on frost occurrence is low  
366 and nearly constant below 3900 m, and then rises gradually above that level. But farther than 10 km

367 away from the salt lake borders, frost occurrence first decreases as elevation rises up to 3900 m and  
368 then increases sharply above. This suggests that thermal inversions at night are more frequent at  
369 distance from the salt lakes. Considering the interaction of elevation with CTI, while frost occurrence at  
370 low elevation increases gradually up to CTI values of 9 and more sharply thereafter (concave  
371 situations), at high elevation the effect of CTI is already important at values below 8 and then rose only  
372 marginally. The effect of landscape concavity thus appears prominent at low elevation, where cold air  
373 can accumulate in local depressions, while it becomes negligible at high elevation where crests and  
374 peaks dominate.



375



376

377 **Fig. 6.** Joint partial dependence plots of some interactions between topographic variables in the  
378 subregional BRT of the January-February period (see Table 1 for variables abbreviations).

379

380 **Table 2.** Validation statistics of frost occurrence multiple regression (MR) and boosted regression trees  
 381 (BRT) models calibrated over the entire study area (regional models) or the Intersalar area (subregional  
 382 models). B: bias; RMSE: root mean square error of prediction; R<sup>2</sup>: determination coefficient of the  
 383 regression line between observed and predicted values. ND = November-December; JF = January-  
 384 February; MA = March-April.

385

Calibration procedure	Period	B	RMSE	R <sup>2</sup>
Regional MR (n = 49353)	ND	2.7 10 <sup>-5</sup>	0.129	0.45
	JF	2.1 10 <sup>-4</sup>	0.093	0.72
	MA	8.5 10 <sup>-4</sup>	0.110	0.59
Regional BRT (n = 49353)	ND	1.7 10 <sup>-5</sup>	0.082	0.78
	JF	0.5 10 <sup>-5</sup>	0.057	0.90
	MA	0.6 10 <sup>-5</sup>	0.071	0.83
Subregional BRT (n = 275)	ND	2.9 10 <sup>-5</sup>	0.062	0.80
	JF	1.4 10 <sup>-3</sup>	0.031	0.82
	MA	2.9 10 <sup>-3</sup>	0.049	0.82

386

### 387 3.3. Fine resolution frost occurrence maps

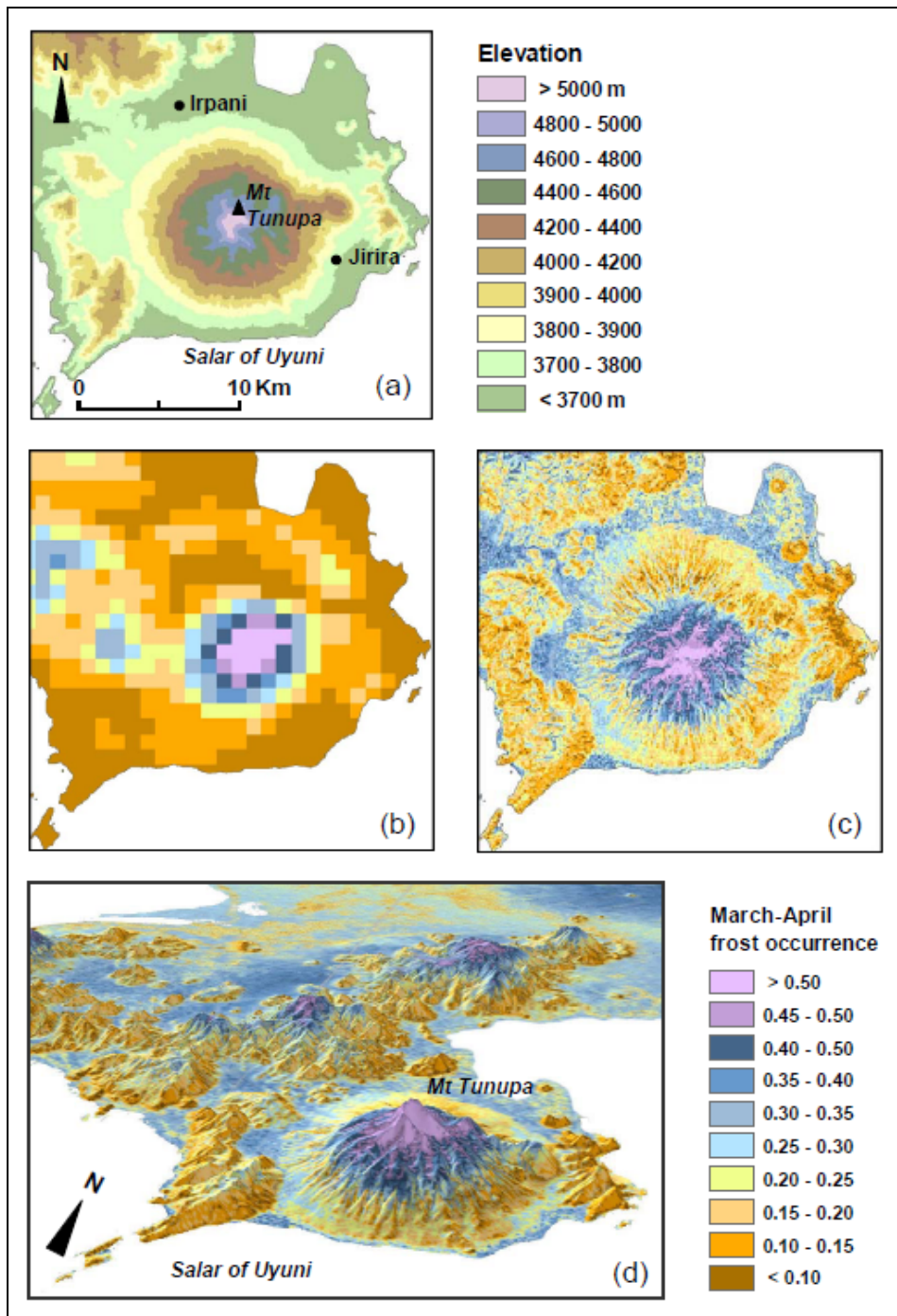
388 Regional BRT were used in prediction to downscale frost occurrence maps from the 1-km to the  
 389 100-m scale. The statistical validation conducted on reaggregated 1-km pixel clusters shows good fit  
 390 between predicted and observed (remotely sensed) frost occurrence values (Table 3), with RMSE of  
 391 predicted values of the same order than in the BRT regional model directly applied at the 1-km  
 392 resolution (Table 2). The 100-m scale maps display topoclimatic variations resulting in a detailed  
 393 zonation of frost occurrence. As an example, Fig. 7c-d shows that flat areas surrounding Mount Tunupa  
 394 are more prone to frost occurrence than the slopes of the volcano up to an elevation of approximately  
 395 4000 m, while sites located at higher altitudes are naturally colder. All over this area, east-facing slopes  
 396 appear less exposed to frost than west-facing slopes. In some particular places at the west, cold air  
 397 stagnation is also identifiable in the lower parts of local depressions. Such details were not visible on  
 398 the 1-km resolution map (Fig. 7b).

399 **Table 3.** Statistical comparison of 100-m frost occurrence predictions reaggregated at 1-km with  
 400 observed 1-km frost occurrence values (n = 49353). B: bias; RMSE: root mean square error of  
 401 prediction; R<sup>2</sup>: determination coefficient of the regression line between observed and predicted values.  
 402 ND = November-December; JF = January-February; MA = March-April.

Period	B	RMSE	R <sup>2</sup>
ND	0.0252	0.0925	0.74
JF	0.0008	0.0644	0.87
MA	0.0543	0.0945	0.80

403





404  
 405 **Fig. 7.** Elevation map of the Mount Tunupa area (a), and frost occurrence in the March-April period  
 406 mapped at 1-km resolution from MODIS observations (b), at 100-m resolution (c) and in 3-D view using  
 407 regional BRT (d). Frost occurrence is scaled between 0 and 1 as the probability of daily occurrence of  
 408 negative  $T_s$  values in the March-April period.

409

410 **3.4. Lapse rate estimation**

411 Table 4 shows significant seasonal variations in the average lapse rate in land surface night  
 412 temperature calculated over the study area, with statistically stronger values in the mid-summer period  
 413 ( $-0.64$  °C/100 m) in comparison with the beginning or the end of the season (ca.  $-0.60$  °C/100 m). The

414 linear relationship between elevation and temperature was also greater in mid-summer compared to the  
415 other two periods. The spatio-temporal variability in lapse rates was high since the coefficients of  
416 variation were between 24 and 35% in the successive time periods, with lower variation in the mid-  
417 summer.

418 **Table 4.** Descriptive statistics of lapse rates of land surface temperature at night in three successive  
419 time periods.

Period	Mean (°C/100 m)	Coefficient of variation (%)	Coefficient of determination	Sample size
November - December	-0.609	35.5	0.50	366
January - February	-0.642	24.3	0.68	355
March - April	-0.598	29.8	0.56	361

420

#### 421 **4. Discussion**

422 The present study provides the first application of MODIS products to characterize frost occurrence  
423 over a 45000 km<sup>2</sup> area in the Andean highlands. Frost occurrence over the summer period was either  
424 calculated directly from land surface temperature remotely sensed at a 1-km scale, or estimated and  
425 downscaled at 100-m by means of physiographic modeling. To our knowledge this is also the first  
426 application of BRT in physiographic modeling. Both techniques are complementary in characterizing  
427 frost occurrence: remote sensing brings spatialized and repetitive information on land surface  
428 temperature and physiographic features, while BRT allow to explore the relative contribution of  
429 physiographic factors at various scales and, hence, to downscale satellite information to a level  
430 appropriate to farming and land management applications.

##### 431 *4.1. Application of remote sensing data for frost occurrence characterization*

432 As pointed by François et al. (1999) at least three factors may potentially affect the relation between  
433 Ts and Tn records: a difference in time (ca. 6 a.m. for minimum night air temperature versus 2 a.m. for  
434 satellite radiative temperature), a difference in height (1.5 m above the soil surface for meteorological  
435 data versus land surface temperature for satellite data), and a difference in spatial resolution (ca. 100  
436 m<sup>2</sup> footprint for local meteorological data versus 1 km<sup>2</sup> for satellite data). In spite of this, these authors  
437 observed only a stable shift of some degrees between Tn records in the Bolivian altiplano and Ts  
438 registered at 2 a.m. with a 1-km spatial resolution by the NOAA/AVHRR satellite. A similar result was  
439 found in the present study showing a linear and highly significant correlation of MODIS land surface  
440 temperature at night with minimum air temperature recorded in meteorological stations ( $R^2 = 0.81$ ).  
441 However, this validation may be biased since, as in most mountain areas in the world, the available  
442 meteorological records are likely not representative of the most elevated and isolated parts of the study  
443 area. Regarding the MODIS satellite, recent studies have improved and validated its calibration  
444 algorithm for land surface temperature in various situations encompassing Bolivian highlands, semiarid  
445 and arid regions, or nighttime/daytime overpasses (Wan, 2008; Wang et al., 2008). This ensures the  
446 reliability of MODIS temperature data in the study area in spite of its specific location in cold and arid  
447 tropical highlands. After verifying for the normality of the distribution of Ts data, the probability of frost

448 occurrence can be easily calculated from the available satellite data series (eq. (1)). It should be noted  
449 that the available series of 6-year daily records was long enough to statistically characterize frost  
450 occurrence at the standard meteorological threshold of 0 °C, but not at lower temperature levels due  
451 the scarcity of observations of severe frost events over the considered period. Frosts at -4 or -7 °C  
452 would, however, be more relevant for agroclimatic purposes since they correspond to the frost tolerance  
453 levels of major Andean crops such as potato and quinoa (Bois et al., 2006; Garcia et al., 2007; Geerts  
454 et al., 2006; Jacobsen et al., 2005). This limitation should progressively disappear as the MODIS  
455 archives grow and allow for the statistical evaluation of less frequent (and more severe) frost events.

#### 456 *4.2. Spatial and temporal patterns of frost occurrence*

##### 457 *4.2.1. Frost occurrence as affected by regional physiography and climate seasonality*

458 The frost occurrence maps derived from MODIS data at 1-km resolution (Fig. 2) clearly show the  
459 influence of regional-scale physiography like the mountain distribution or the proximity of the salt lakes,  
460 as well as the seasonal variation of frost occurrence over a 6-month period. In their attempt to map  
461 agroclimatic suitability in the Bolivian altiplano, Geerts et al. (2006) notice that frost risk is difficult to  
462 interpolate spatially. Nevertheless, based on data from 41 ground climatic stations of the altiplano, they  
463 achieve a description of regional frost risk patterns that are globally confirmed by our satellite maps,  
464 with lower frost probabilities in the Intersalar region and higher probabilities at the south-west of the salt  
465 lake of Uyuni. Geerts et al. (2006) also mention that their kriging interpolation was improved by  
466 incorporating a WNW anisotropy due to the combined north-south influence of the Lake Titicaca and the  
467 west-east effect of zonal winds. These zonal winds affect the entire altiplano and largely control the  
468 synoptic weather types (Garreaud et al., 2003). As demonstrated in other cold regions or mountain  
469 areas in the world (Blandford et al., 2008; Dobrowski et al., 2009; Marshall et al., 2007), the occurrence  
470 and spatial patterns of the zonal winds could be important drivers of the seasonal variation in land  
471 surface temperature and temperature lapse rate found in the study area.

472 Another driver of frost seasonality is cloud cover which, in a typical tropical unimodal rainy season,  
473 results in progressive overcasting at the beginning of the rainy season, maximum cloud cover in the  
474 mid-season, and then progressive decrease by the end of the season. This cloud cover pattern is  
475 recorded daily at the 1-km scale by the MODIS satellite and was integrated in the calculation and  
476 mapping of frost occurrence (equation 1, Fig. 2).

477 The seasonal change in sky cloudiness also influences temperature lapse rates. Blandford et al.  
478 (2008) thoroughly discuss the effect of seasonal and synoptic conditions on lapse rate calculated for  
479 average or daily extreme values of near-ground temperature in temperate mountains. They outlined that  
480 minimum temperature lapse rate are shallower when air masses are dry and cold, which is explained by  
481 increased frequency of cold air drainage and temperature inversions under clear-sky and dry air  
482 conditions at night. Minimum temperature lapse rate values are also more variable during seasonal  
483 transition between summer and winter, due to fluctuating weather regime at that time and higher  
484 frequency of temperature inversions. Our estimates of minimum temperature lapse rate in successive  
485 time periods (Table 4) are consistent with both assertions, showing steeper and less variable values in  
486 mid-summer (January-February) when the sky is more cloudy and air conditions are relatively humid,

487 temperate, and stable. These estimates approximating  $-0.6\text{ }^{\circ}\text{C}/100\text{ m}$  appear fairly high compared to  
488 minimum temperature lapse rate values, typically ranging from  $-0.15$  to  $-0.35\text{ }^{\circ}\text{C}/100\text{ m}$ , in mountains  
489 of mid-latitude regions (Blandford et al., 2008; Dobrowski et al., 2009; Harlow et al., 2004). In  
490 subtropical mountains however, De Scally (1997 ) states that, due to their high thermal regime, the  
491 temperature lapse rate is generally higher than in mid-latitude mountains. The high lapse rate values  
492 thus quoted for the Himalaya (De Scally, 1997 ) or the Andes (Frère et al., 1978; Snow, 1975 cited by  
493 Pielke & Mehring, 1977; Trombotto et al., 1997) refer unfortunately to mean daily or mean annual  
494 temperatures which cannot be compared directly to our estimates of minimum temperature lapse rates  
495 in specific time periods.

496 Astronomic forcing is another cause of seasonality in the topography-frost relationship, explaining  
497 why topographic controls, usually treated as stationary, show actually pronounced seasonal variations,  
498 as pointed by Deng et al. (2007) in the case of topography-vegetation relationships. In our study,  
499 seasonal changes in the effects of slope steepness and aspect on frost occurrence are illustrated by  
500 varying SLO and DPI contributions (Fig. 4b). They are explained by astronomical forcing resulting in  
501 insolation values in the early and mid-summer higher by 25% in average than in the late-summer period  
502 (see Table 1), thus giving higher influence of DPI over SLO in the former two periods.

503 Fig. 2 shows that the shores of the salt lakes are less prone to frost, while highlands at the west  
504 and south of the region are continuously exposed, even in mid-summer (January-February) when frost  
505 occurrence is generally low. This latter situation is obviously due to extreme elevation, while the  
506 "milding" effect of the salt lakes could be due to the specific thermal properties of these vast salted  
507 extenses. François et al. (1999) observed warmer night temperatures over the Coipasa and Uyuni salt  
508 lakes and suggest that water covering these lakes part of the summer, as well as the higher thermal  
509 conductivity and thermal capacity of the salted substratum, could explain that their borders remain  
510 warmer than the surrounding areas.

#### 511 *4.2.2. From regional to subregional physiographic influences on frost occurrence*

512 Multiple regression methods were used in previous studies to evaluate the relative contribution of  
513 topographic factors to near-ground temperature and frost occurrence. These studies were generally  
514 conducted in mid- or high-latitude mountains (Bennie et al., 2009; Chuanyan et al., 2005; Dobrowski et  
515 al., 2009), and often in densely forested areas at mid-altitude (Blennow, 1998; Lindkvist et al., 2000;  
516 Pypker et al., 2007b). Our study explored an extended agricultural region at its extreme elevation limit in  
517 cold and arid tropical highlands. In this context, BRT models clearly outperformed multiple regression  
518 models, probably due to their capacity to include nonlinear effects and interactions between predictors  
519 (Martin et al., 2009). At the regional scale, BRT analyses show that elevation, distance to the salt lakes  
520 and latitude were the physiographic features most contributing to frost occurrence variations, while  
521 features directly or indirectly related to slope or topographic convergence (SLO, CTI, DPI, API, and  
522 MPI) were less important. These regional BRT models based on physiographic features alone explain  
523 between 78% and 90% of the variation in frost occurrence observed in different time periods (Table 2).  
524 In their study of the influence of physiography on the distribution of climate variables across the United  
525 States, Daly et al. (2008) outline that the effects of elevation and proximity to large water bodies exceed

526 those of other topographic factors at large scales, whereas the effects of slope and landcover features  
527 become prominent at relatively smaller scales. In complex terrains, local variations in slope aspect and  
528 steepness create a mosaic of hillslopes experiencing contrasting climatic regimes (Daly et al., 2008),  
529 while topographic depressions are another landscape feature commonly associated with cold air  
530 drainage and frost occurrence (Lundquist et al., 2008; Pypker et al., 2007b). These local landform  
531 features emerge as forcing factors of frost occurrence at the local scale, where the range of variation in  
532 elevation and latitude became limited while that in local landscape features remained large. When  
533 applied to the reduced spatial domain of the *Intersalar*, our BRT analyses indeed showed that elevation  
534 lost some importance at the benefit of daily potential insolation (DPI), slope steepness (SLO), or  
535 topographic convergence (CTI) (Fig. 4b). As a major characteristic of the physiography of south-  
536 western Bolivia, the vast salt lakes of Coipasa and Uyuni remained influential at that local scale, as  
537 shown by the high contribution of the distance to the salt lakes (LDS) in these BRT subregional models.  
538 The good fit of frost occurrence values predicted by BRT models applied either at the 100-m or the 1-  
539 km resolution (Tables 2 and 3) validates the use of BRT regional models for local frost occurrence  
540 estimations since these models were able to seize both the influences of large-scale factors like latitude  
541 and elevation, and of local factors like slope steepness, insolation, and landscape position. The  
542 resulting local mosaic of cold depressions and warmer slopes at particular elevations and exposures is  
543 illustrated by the map in Fig. 7c. We hypothesized that small-scale variations in soil warming due to  
544 differential insolation in the day before (or the morning after) a given night could influence soil cooling  
545 and thus radiative frost at night in particular places. In fact, the contribution of DPI appeared significant  
546 in the BRT subregional model, at least from November to February when potential insolation is at its  
547 seasonal maximum (Table 1), thus leading to highest contrasts in soil energy balance between sunlit  
548 and shaded locations. However, the small contributions of the afternoon or morning components of  
549 insolation (API and MPI) (Fig. 4b) seem to belie the idea that potential insolation is directly involved in  
550 frost vulnerability at particular places. Actually, Blennow (1998) states that the larger amount of heat  
551 stored into the ground in sunlit places cannot compensate for soil cooling at night since this cooling  
552 occurs within a few hours after sunset. Nocturnal soil cooling should be still faster under clear-sky  
553 conditions at high altitude. This is, however, in contradiction with the common perception of lower frost  
554 occurrence in sunlit slopes, particularly in stony terrains and shallow soils supposed to benefit from the  
555 thermal stability provided by the rocks. Microclimate stability associated to rock outcrops has been  
556 documented by Rada et al. (2009) in the *paramo* ecosystem of Venezuelan Andes at lower elevation  
557 (3800 m) and under wetter conditions (969 mm of annual precipitation). It is likely that the much drier  
558 conditions of the *puna* ecosystem in southern Bolivia reduce the thermal inertia of the soils, thus leading  
559 to a very fast soil cooling at night. Apart from astronomical forcing discussed previously, the varying  
560 importance of CTI, DPI and SLO in the BRT models, as well as the interactions between them (Fig. 6)  
561 reflect complex spatio-temporal relations between insolation and landform factors producing  
562 multiplicative or mitigating effects on near-ground temperature. At the microscale level, unobserved soil  
563 and vegetation properties might also interfere with landform features. Soil moisture and vegetation  
564 cover, for example, are known to influence the radiative balance at the soil surface, and might  
565 contribute to buffer the near-ground temperature from cold extremes in particular places (Fridley, 2009;  
566 Geiger, 1971).

567 *4.3. Ecological implications*

568 The relationships between ecological patterns and processes change across spatial and temporal  
569 scales, with singular complexity in mountain areas (e.g., Deng et al., 2007; Saunders et al., 1998).  
570 Regarding air or soil surface temperature in mountains, nested factors are interacting, from regional  
571 synoptic weather forcing to local topoclimatic situations and microscale variations in vegetation cover  
572 and soil moisture. All these factors in turn may dominate the distribution of temperatures, depending not  
573 only on the dynamics of the situation (turbulent or stable, nighttime or daytime conditions...) but also on  
574 the spatial and temporal scale of interest (from macroscale to microscale, from seasonal to  
575 instantaneous). In this way, macroscale conditions of clear sky and calm nights are required for  
576 radiative frost to occur, but the frequency and severity of these frost events are further increased by low  
577 site position (or conversely, extremely high location) and, at still smaller scales, by vegetation  
578 sparseness and soil surface dryness or roughness (De Chantal et al., 2007; Fridley 2009; Langvall &  
579 Ottonson Löfvenius, 2002; Oke, 1970). In the Andean highlands, instantaneous near-ground minimum  
580 temperature may be 4°C lower in a sparsely vegetated area compared to a neighboring forest  
581 understory (Rada et al., 2009). Similar fine scale variations in minimum air temperature occur within  
582 cultivated canopies despite the low plant cover of most Andean crop species (see Winkel et al., 2009,  
583 for the quinoa crop). These local variations in minimum near-ground temperatures may be sufficient for  
584 some part of the vegetation to escape lethal freezing. Potential frost impacts on vegetation operating at  
585 regional and subregional scales may thus be over-shadowed by microscale variability in minimum  
586 temperature. Yet, contrary to what occurs in dense forests where plant interactions within canopies are  
587 significant (Bader et al., 2008; Turnipseed et al., 2003), the sparse and low vegetation typical of the  
588 Andean highlands is likely to exert an influence limited to small spatial scales, with topography and  
589 coarse scale factors controlling most of the variation in minimum air temperature. In fact, Blennow  
590 (1998) outlines that topographic influences on minimum air temperature increase in parallel with  
591 decreasing vegetation cover.

592 *4.4. Practical implications*

593 The latter consideration implies that agroclimatic applications, such as crop zonation or suitability  
594 assessments, require a multi-scale approach, ideally complementing frost risk characterization at the  
595 topoclimatic scale by an evaluation of the local effects of crop practices on canopy structure and soil  
596 surface moisture and roughness. Though limited to topography-frost relationships, our attempt of  
597 downscaling frost occurrence at a 100-m scale usefully expands previous works on regional  
598 agroclimatic zoning in the Bolivian altiplano (François et al., 1999; Geerts et al., 2006). To our  
599 knowledge, this is the first time that such a detailed zonation of topoclimate is reported for this region,  
600 providing fine-scale information helpful for land management and rural planning (Theobald et al., 2005).  
601 Considering the scarcely available meteorological records in the study area, these 100-m scale maps  
602 bring new information about the spatio-temporal variation of frost occurrence, allowing now to localize  
603 exactly the seasonal pattern of frost typical of the Andean summer period (Frère et al., 1978; Troll,  
604 1968). For instance, the virtual zero value of frost frequency in January and February derived from  
605 meteorological records at Salinas (Fig. 1), covers in reality a wide range of situations with still significant  
606 frost occurrence in mid-summer, as on the nearby border of the salar of Coipasa or the western and

607 southern part of the study area (Fig. 2). In fact, the recent expansion of quinoa crop in the region was  
608 firstly and mostly located in flat areas near the Coipasa and Uyuni salt lakes (Vassas et al., 2008),  
609 which exemplifies the complex trade-offs between agroclimatic risks and economic expectancies  
610 operating in farmers' decision making (Luers 2005; Sadras et al., 2003).

#### 611 4.5. Perspectives

612 Through remote sensing of land surface temperature and modeling of topographic features  
613 implemented within a boosted regression procedure, we were able to explicitly downscale frost  
614 occurrence at the landscape scale. The method developed here may be adapted to climatic or  
615 ecological processes other than frost. Rainfall distribution could be a candidate since its spatio-temporal  
616 patterns clearly depends on landscape characteristics over complex terrains. Current literature outlines  
617 the importance of landform as a factor of rainfall variability in the Andes (Giovannettone & Barros,  
618 2009), though most studies were conducted at the coarse spatial resolution appropriate to continental  
619 scale climatology (Garreaud & Aceituno, 2001; Misra et al., 2003; Vuille et al., 2003). Canopy energy  
620 budget, soil water balance, or ecosystem productivity are other ecological processes tractable for  
621 topographic modeling (Bradford et al., 2005; Rana et al., 2007; Urban et al., 2000). Such applications  
622 depend firstly on the availability of remotely sensed proxies for the considered process. For example,  
623 the remotely sensed daily amplitude in surface temperature and vegetation indices can be used to  
624 derive daily evapotranspiration (Wang et al., 2006). Similarly, satellite estimates of absorbed  
625 photosynthetically active radiation may serve to evaluate net primary productivity (Bradford et al., 2005;  
626 Turner et al., 2009). An additional requisite for the calibration of these applications consists in local  
627 ground measurements for the variable of interest. This is a major issue in the case of the tropical  
628 highlands where, similarly to what occurs for meteorological data, reliable datasets on matter and  
629 energy fluxes at ground level are and will remain scarce (Vergara et al., 2007). The methods and  
630 results presented here can contribute to a better understanding of the potential risks associated with  
631 climate and land use changes in complex terrains, so that decision-makers can develop efficient  
632 strategies to improve the ecological sustainability of natural and agricultural ecosystems in vulnerable  
633 mountain areas.

#### 634 Acknowledgements

635 The authors are most grateful to Danny Lo Seen (Cirad, France) for discussions on BRT methods.  
636 They also acknowledge the comments made by the anonymous reviewers of the paper. This work was  
637 carried out with the financial support of the ANR (Agence Nationale de la Recherche - The French  
638 National Research Agency) under the Programme "Agriculture et Développement Durable", project  
639 "ANR-06-PADD-011-EQUECO".

#### 640 References

- 641 Bader, M.Y., Rietkerk, M., & Bregt, A.K. (2008). A simple spatial model exploring positive feedbacks at  
642 tropical alpine treelines. *Arctic, Antarctic, and Alpine Research*, 40, 269-278.
- 643 Bader, M.Y., & Ruijten, J.J.A. (2008). A topography-based model of forest cover at the alpine tree line in  
644 the tropical Andes. *Journal of Biogeography*, 35, 711-723.

645 Benavides, R., Montes, F., Rubio, A., & Osoro, K. (2007). Geostatistical modelling of air temperature in  
646 a mountainous region of Northern Spain. *Agricultural and Forest Meteorology*, 146, 173-188.

647 Bennie, J.J., Wiltshire, A.J., Joyce, A.N., Clark, D., Lloyd, A.R., Adamson, J., Parr, T., Baxter, R., &  
648 Huntley, B. (2009). Characterising inter-annual variation in the spatial pattern of thermal microclimate in  
649 a UK upland using a combined empirical-physical model. *Agricultural and Forest Meteorology*, 150, 12-  
650 19.

651 Blandford, T.R., Humes, K.S., Harshburger, B.J., Moore, B.C., Walden, V.P., & Ye, H. (2008). Seasonal  
652 and synoptic variations in near-surface air temperature lapse rates in a mountainous basin. *Journal of*  
653 *Applied Meteorology and Climatology*, 47, 249-261.

654 Blennow, K. (1998). Modelling minimum air temperature in partially and clear felled forests. *Agricultural*  
655 *and Forest Meteorology*, 91, 223-235.

656 Blennow, K., & Lindkvist, L. (2000). Models of low temperature and high irradiance and their application  
657 to explaining the risk of seedling mortality. *Forest Ecology and Management*, 135, 289-301.

658 Bois, J.F., Winkel, T., Lhomme, J.P., Raffaillac, J.P., & Rocheteau, A. (2006). Response of some  
659 Andean cultivars of quinoa (*Chenopodium quinoa* Willd.) to temperature: effects on germination,  
660 phenology, growth and freezing. *European Journal of Agronomy*, 25, 299-308.

661 Bradford, J.B., Hicke, J.A., & Lauenroth, W.K. (2005). The relative importance of light-use efficiency  
662 modifications from environmental conditions and cultivation for estimation of large-scale net primary  
663 productivity. *Remote Sensing of Environment*, 96, 246-255.

664 Chen, J., Saunders, S.C., Crow, T.R., Naiman, R.J., Brososke, K.D., Mroz, G.D., Brookshire, B.L., &  
665 Franklin, J.F. (1999). Microclimate in forest ecosystem and landscape ecology. *Bioscience*, 49, 288-  
666 297.

667 Chuanyan, Z., Zhongren, N., & Guodong, C. (2005). Methods for modelling of temporal and spatial  
668 distribution of air temperature at landscape scale in the southern Qilian mountains, China. *Ecological*  
669 *Modelling*, 189, 209-220.

670 Daly, C., Halbleib, M., Smith, J.I., Gibson, W.P., Doggett, M.K., Taylor, G.H., Curtis, J., & Pasteris, P.P.  
671 (2008). Physiographically sensitive mapping of climatological temperature and precipitation across the  
672 conterminous United States. *International Journal of Climatology*, 28, 2031-2064.

673 De Chantal, M., Hanssen, K.H., Granhus, A., Bergsten, U., Lofvenius, M.O., & Grip, H. (2007). Frost-  
674 heaving damage to one-year-old *Picea abies* seedlings increases with soil horizon depth and canopy  
675 gap size. *Canadian Journal of Forest Research*, 37, 1236-1243.

676 De Scally, F.A. (1997 ). Deriving lapse rates of slope air temperature for meltwater runoff modeling in  
677 subtropical mountains: an exemple from the Punjab Himalaya. *Moutain Research and Development*,  
678 17, 353-362.

679 Del Castillo, C., Mahy, G., & Winkel, T. (2008). Quinoa in Bollivia: an ancestral crop changed to a cash  
680 crop with "organic fair-trade" labeling. *Biotechnologie, Agronomie, Société et Environnement (BASE)*,  
681 12, 421-435.



682 Deng, Y., Chen, X., Chuvieco, E., Warner, T., & Wilson, J.P. (2007). Multi-scale linkages between  
683 topographic attributes and vegetation indices in a mountainous landscape. *Remote Sensing of*  
684 *Environment*, 111, 122-134.

685 Dobrowski, S.Z., Abatzoglou, J.T., Greenberg, J.A., & Schladow, S.G. (2009). How much influence  
686 does landscape-scale physiography have on air temperature in a mountain environment? *Agricultural*  
687 *and Forest Meteorology*, 149, 1751-1758.

688 Elith, J., Leathwick, J.R., & Hastie, T. (2008). A working guide to boosted regression trees. *Journal of*  
689 *Animal Ecology*, 77, 802-813.

690 Farr, T.G., Rosen, P.A., Caro, E., Crippen, R., Duren, R., Hensley, S., Kobrick, M., Paller, M.,  
691 Rodriguez, E., Roth, L., Seal, D., Shaffer, S., Shimada, J., Umland, J., Werner, M., Oskin, M., Burbank,  
692 D., & Alsdorf, D. (2007). The shuttle radar topography mission. *Reviews of Geophysics*, 45, RG2004,  
693 doi: 2010.1029/2005RG000183.

694 François, C., Bosseno, R., Vacher, J.J., & Seguin, B. (1999). Frost risk mapping derived from satellite  
695 and surface data over the Bolivian Altiplano. *Agricultural and Forest Meteorology*, 95, 113-137.

696 Frère, M., Rijks, J.Q., & Rea, J. (1978). *Estudio agroclimatológico de la zona andina. Nota Técnica n°*  
697 *161*. (373 p.). Ginebra, Suiza: Proyecto interinstitucional FAO/UNESCO/OMM. Organización  
698 Meteorológica Mundial.

699 Fridley, J.D. (2009). Downscaling climate over complex terrain: high finescale (<1000 m) spatial  
700 variation of near-ground temperatures in a montane forested landscape (Great Smoky Mountains).  
701 *Journal of Applied Meteorology and Climatology*, 48, 1033-1049.

702 Friedman, J.H., & Meulman, J.J. (2003). Multiple additive regression trees with application in  
703 epidemiology. *Statistics in Medicine*, 22, 1365-1381.

704 Fu, P., & Rich, P.M. (2002). A geometric solar radiation model with applications in agriculture and  
705 forestry. *Computers and Electronics in Agriculture*, 37, 25-35.

706 Garcia, M., Raes, D., Allen, R., & Herbas, C. (2004). Dynamics of reference evapotranspiration in the  
707 Bolivian highlands (Altiplano). *Agricultural and Forest Meteorology*, 125, 67-82.

708 Garcia, M., Raes, D., Jacobsen, S.E., & Michel, T. (2007). Agroclimatic constraints for rainfed  
709 agriculture in the Bolivian Altiplano. *Journal of Arid Environments*, 71, 109-121.

710 Garreaud, R., Vuille, M., & Clement, A.C. (2003). The climate of the Altiplano: observed current  
711 conditions and mechanisms of past changes. *Palaeogeography, Palaeoclimatology, Palaeoecology*,  
712 194 5-22.

713 Garreaud, R.D., & Aceituno, P. (2001). Interannual rainfall variability over the South American altiplano.  
714 *Journal of Climate*, 14, 2779-2789.

715 Geerts, S., Raes, D., Garcia, M., Del Castillo, C., & Buytaert, W. (2006). Agro-climatic suitability  
716 mapping for crop production in the Bolivian Altiplano: a case study for quinoa. *Agricultural and Forest*  
717 *Meteorology*, 139, 399-412.

718 Geiger, R. (1971). *The climate near the ground*. Cambridge, MA, USA: Harvard University Press.

719 Gessler, P.E., Chadwick, O.A., Chamran, F., Althouse, L., & Holmes, K. (2000). Modeling soil-  
720 landscape and ecosystem properties using terrain attributes. *Soil Science Society of America Journal*,  
721 64, 2046-2056.

722 Giovannettone, J.P., & Barros, A.P. (2009). Probing regional orographic controls of precipitation and  
723 cloudiness in the central Andes using satellite data. *Journal of Hydrometeorology*, 10, 167-182.

724 Gonzalez, J.A., Gallardo, M.G., Boero, C., Liberman Cruz, M., & Prado, F.E. (2007). Altitudinal and  
725 seasonal variation of protective and photosynthetic pigments in leaves of the world's highest elevation  
726 trees *Polylepis tarapacana* (Rosaceae). *Acta Oecologica*, 32, 36-41.

727 Grötzbach, E., & Stadel, C. (1997). Mountain peoples and cultures. In B. Messerli & J.D. Ives (Eds.),  
728 *Mountains of the world: a global priority* (pp. 17-38). New York, USA: The Partenon Publishing Group.

729 Harlow, R.C., Burke, E.J., Scott, R.L., Shuttleworth, W.J., Brown, C.M., & Petti, J.R. (2004). Derivation  
730 of temperature lapse rates in semi-arid south-eastern Arizona. *Hydrology and Earth System Sciences*,  
731 8, 1179-1185.

732 Hoch, G., & Körner, C. (2005). Growth, demography and carbon relations of *Polylepis* trees at the  
733 world's highest treeline. *Functional Ecology*, 19, 941-951.

734 Jacobsen, S.E., Monteros, C., Christiansen, J.L., Bravo, L.A., Corcuera, L.J., & Mujica, A. (2005). Plant  
735 responses of quinoa (*Chenopodium quinoa* Willd.) to frost at various phenological stages. *European*  
736 *Journal of Agronomy*, 22, 131-139.

737 Langvall, O., & Ottonson Löfvenius, M. (2002). Effect of shelterwood density on nocturnal near-ground  
738 temperature, frost injury risk and budburst date of Norway spruce. *Forest Ecology and Management*,  
739 168, 149-161.

740 Lawrence, R., Bunn, A., Powell, S., & Zambon, M. (2004). Classification of remotely sensed imagery  
741 using stochastic gradient boosting as a refinement of classification tree analysis. *Remote Sensing of*  
742 *Environment*, 90, 331-336.

743 Lindkvist, L., Gustavsson, T., & Bogren, J. (2000). A frost assessment method for mountainous areas.  
744 *Agricultural and Forest Meteorology*, 102, 51-67.

745 Lookingbill, T.R., & Urban, D.L. (2003). Spatial estimation of air temperature differences for landscape-  
746 scale studies in montane environments. *Agricultural and Forest Meteorology*, 114, 141-151.

747 Luers, A.L. (2005). The surface of vulnerability: an analytical framework for examining environmental  
748 change. *Global Environmental Change Part A*, 15, 214-223.

749 Lundquist, J.D., Pepin, N., & Rochford, C. (2008). Automated algorithm for mapping regions of cold-air  
750 pooling in complex terrain. *Journal of Geophysical Research*, 113, D22107 doi:  
751 22110.21029/22008JD009879.

752 Marshall, S.J., Sharp, M.J., Burgess, D.O., & Anslow, F.S. (2007). Near-surface-temperature lapse  
753 rates on the Prince of Wales Icefield, Ellesmere Island, Canada: implications for regional downscaling  
754 of temperature. *International Journal of Climatology*, 27, 385-398.

755 Martin, M.P., Lo Seen, D., Boulonne, L., Jolivet, C., Nair, K.M., Bourgeon, G., & Arrouays, D. (2009).  
756 Optimizing pedotransfer functions for estimating soil bulk density using boosted regression trees. *Soil*  
757 *Science Society of America Journal*, 73, 485-493.

758 Misra, V., Dirmeyer, P.A., & Kirtman, B.P. (2003). Dynamic downscaling of seasonal simulations over  
759 South America. *Journal of Climate*, 16, 103-117.

760 Nagy, L., Grabherr, G., Körner, C., & Thompson, D.B.A. (Eds.) (2003). *Alpine biodiversity in Europe*.  
761 Berlin, Germany: Springer Verlag.

762 Navarro, G., & Ferreira, W. (2007). *Mapa de vegetación de Bolivia a escala 1:250.000*. Santa Cruz de  
763 la Sierra, Bolivia: The Nature Conservancy (TNC)

764 Oke, T.R. (1970). The temperature profile near the ground on calm clear nights. *Quarterly Journal of the*  
765 *Royal Meteorological Society*, 96, 14-23.

766 Parisien, M.-A., & Moritz, M.A. (2009). Environmental controls on the distribution of wildfire at multiple  
767 spatial scales. *Ecological Monographs*, 79, 127-154.

768 Pielke, R.A., & Mehring, P. (1977). Use of mesoscale climatology in mountainous terrain to improve  
769 spatial representation of mean monthly temperatures. *Monthly Weather Review*, 105, 108-112.

770 Pypker, T.G., Unsworth, M.H., Lamb, B., Allwine, E., Edburg, S., Sulzman, E., Mix, A.C., & Bond, B.J.  
771 (2007a). Cold air drainage in a forested valley: investigating the feasibility of monitoring ecosystem  
772 metabolism. *Agricultural and Forest Meteorology*, 145, 149-166.

773 Pypker, T.G., Unsworth, M.H., Mix, A.C., Rugh, W., Ocheltree, T., Alstad, K., & Bond, B.J. (2007b).  
774 Using nocturnal cold air drainage flow to monitor ecosystem processes in complex terrain. *Ecological*  
775 *Applications*, 17, 702-714.

776 R Development Core Team (2006). *R: a language and environment for statistical computing*. Vienna,  
777 Austria: R Foundation for Statistical Computing.

778 Rada, F., García-Núñez, C., & Rangel, S. (2009). Low temperature resistance in saplings and ramets of  
779 *Polylepis sericea* in the Venezuelan Andes. *Acta Oecologica*, 35, 610-613.

780 Rana, G., Ferrara, R.M., Martinelli, N., Personnic, P., & Cellier, P. (2007). Estimating energy fluxes from  
781 sloping crops using standard agrometeorological measurements and topography. *Agricultural and*  
782 *Forest Meteorology*, 146, 116-133.

783 Ronchail, J. (1989). Advections polaires en Bolivie : mise en évidence et caractérisation des effets  
784 climatiques. *Hydrologie Continentale*, 4, 49-56.

785 Sadras, V., Roget, D., & Krause, M. (2003). Dynamic cropping strategies for risk management in dry-  
786 land farming systems. *Agricultural Systems*, 76, 929-948.

787 Santibañez, F., Morales, L., de la Fuente, J., Cellier, P., & Huete, A. (1997). Topoclimatic modeling for  
788 minimum temperature prediction at a regional scale in the Central Valley of Chile. *Agronomie*, 17, 307-  
789 314.

790 Saunders, S.C., Chen, J.Q., Crow, T.R., & Brosofske, K.D. (1998). Hierarchical relationships between  
791 landscape structure and temperature in a managed forest landscape. *Landscape Ecology*, 13, 381-395.

792 StatSoft France (2005). *STATISTICA (logiciel d'analyse de données), version 7.1: [www.statsoft.fr](http://www.statsoft.fr)*

793 Snow, J. W. (1975). *The climates of northern South America*. M.Sc. Thesis, University of Wisconsin,  
794 Madison. 238 pp.

795 Theobald, D.M., Spies, T., Kline, J., Maxwell, B., Hobbs, N.T., & Dale, V.H. (2005). Ecological support  
796 for rural land-use planning. *Ecological Applications*, 15, 1906-1914.

797 Troll, C. (1968). The Cordilleras of the tropical Americas: aspects of climatic, phytogeographical and  
798 agrarian ecology. In C. Troll (Ed.), *Proceedings of the UNESCO Mexico Symposium, August 1-3 1966*.  
799 *Colloquium Geographicum, vol.9* (pp. 15-56). Bonn, Germany: Ferd. Dümmlers Verlag.

800 Trombotto, D., Buk, E., & Hernández, J. (1997). Monitoring of mountain permafrost in the Central  
801 Andes, Cordon del Plata, Mendoza, Argentina. *Permafrost and Periglacial Processes*, 8, 123-129.

802 Turner, D.P., Ritts, W.D., Wharton, S., Thomas, C., Monson, R., Black, T.A., & Falk, M. (2009).  
803 Assessing FPAR source and parameter optimization scheme in application of a diagnostic carbon flux  
804 model. *Remote Sensing of Environment*, 113, 1529-1539.

805 Turnipseed, A.A., Anderson, D.E., Blanken, P.D., Baugh, W.M., & Monson, R.K. (2003). Airflows and  
806 turbulent flux measurements in mountainous terrain: Part 1. Canopy and local effects. *Agricultural and*  
807 *Forest Meteorology*, 119, 1-21.

808 Urban, D., Miller, C., Halpin, P., & Stephenson, N. (2000). Forest gradient response in Sierran  
809 landscapes: the physical template. *Landscape Ecology*, 15, 603-620.

810 Vassas, A., Vieira Pak, M., & Duprat, J.R. (2008). El auge de la quinua: cambios y perspectivas desde  
811 una visión social. *Habitat*, 75: 31-35.

812 Vergara, W., Kondo, H., Pérez Pérez, E., Méndez Pérez, J.M., Magaña Rueda, V., Martínez Arango,  
813 M.C., Ruíz Murcia, J.F., Avalos Roldán, G.J., & Palacios, E. (2007). Visualizing Future Climate in Latin  
814 America: results from the application of the Earth Simulator. In (p. 82 p.): The World Bank, Latin  
815 America and the Caribbean Region

816 Vuille, M., Bradley, R.S., Werner, M., & Keimig, F. (2003). 20th century climate change in the tropical  
817 Andes: observations and model results. *Climatic Change*, 59, 75-99.

818 Vuille, M., Francou, B., Wagnon, P., Juen, I., Kaser, G., Mark, B.G., & Bradley, R.S. (2008). Climate  
819 Change and tropical Andean glaciers: past, present and future. *Earth-Science Reviews*, 89, 79-96.

820 Wan, Z. (2008). New refinements and validation of the MODIS Land-Surface Temperature/Emissivity  
821 products. *Remote Sensing of Environment*, 112, 59-74.

- 822 Wang, K., Li, Z., & Cribb, M. (2006). Estimation of evaporative fraction from a combination of day and  
823 night land surface temperatures and NDVI: a new method to determine the Priestley-Taylor parameter.  
824 *Remote Sensing of Environment*, 102, 293-305.
- 825 Wang, W., Liang, S., & Meyers, T. (2008). Validating MODIS land surface temperature products using  
826 long-term nighttime ground measurements. *Remote Sensing of Environment*, 112, 623-635.
- 827 Winkel, T., Lhomme, J.P., Nina Laura, J.P., Mamani Alcón, C., Del Castillo, C., & Rocheteau, A. (2009).  
828 Assessing the protective effect of vertically heterogeneous canopies against radiative frost: the case of  
829 quinoa on the Andean Altiplano. *Agricultural and Forest Meteorology*, 149, 1759-1768.